frontiers | Frontiers in Earth Science

TYPE Original Research
PUBLISHED 16 September 2022
DOI 10.3389/feart.2022.953152

OPEN ACCESS

EDITED BY
Nobuo Geshi,
Geological Survey of Japan (AIST), Japan

REVIEWED BY
Laura Pioli,
University of Cagliari, Italy
Shimpei Uesawa,
Central Research Institute of Electric Power Industry (CRIEPI), Japan

*CORRESPONDENCE
Takeshi Hasegawa,
takeshi.hasegawa.paul@vc.ibaraki.ac.jp

SPECIALTY SECTION
This article was submitted to Volcanology, a section of the journal Frontiers in Earth Science

RECEIVED 25 May 2022
ACCEPTED 25 August 2022
PUBLISHED 16 September 2022

CITATION
Hasegawa T, Nakagawa M, Kamiyama H and Yamamoto A (2022), Geological, geophysical, and geochemical constraints on the time-space evolution of Akan composite caldera, Hokkaido, Japan.
Front. Earth Sci. 10:953152.
doi: 10.3389/feart.2022.953152

Geological, geophysical, and geochemical constraints on the time-space evolution of Akan composite caldera, Hokkaido, Japan

Takeshi Hasegawa[1]*, Mitsuhiro Nakagawa[2], Hiroyuki Kamiyama[3] and Akihiko Yamamoto[4]

[1]Department of Earth Sciences, College of Science, Ibaraki University, Mito, Japan, [2]Department of Natural History Sciences, Graduate School of Science, Hokkaido University, Sapporo, Japan, [3]Ueyama-Shisui Co., Ltd, Sapporo, Japan, [4]Department of Earth's Evolution and Environment, Graduate School of Science and Engineering, Ehime University, Matsuyama, Japan

Some calderas are geometrically complex that may be related not to a single eruption, magma body, or structure. In order to reveal their forming processes, multidisciplinary methods should be applied. Akan volcano has E-W elongated and irregular-shaped caldera (24 × 13 km), implying a complex mechanism of formation. Akan caldera results from successive explosive eruptions from 1.4 to 0.1 Ma. On the basis of duration of dormancy and petrological features (mainly whole-rock major element compositions) of juvenile materials, these eruptions have been grouped into 17 eruptive groups (Ak1–Ak17), each of which consists of a single or a sequential phase. In order to investigate the processes of caldera formation, we focus on the younger eruptive groups (Ak1–Ak7: 0.8 to 0.2 Ma) that have relatively large magnitudes (>10 km^3) and likely control the present caldera shape. We performed component analysis of lithic fragments from pyroclastic fallout deposits, whole-rock trace element analysis of juveniles, and gravitational survey of the caldera. We grouped Ak1–Ak7 into three types, namely, type A (Ak1, Ak2), type B (Ak3–Ak5), and type C (Ak6, Ak7), based on the lithic componentry, most of which are accessary and accidental fragments from vent and conduit areas. The characteristic lithic component in each type is as follows: altered rock in type A, aphyric dacite in type B, and pyroxene andesite in type C. These data suggest that explosive eruptions of each type are derived from distinct sources. The whole-rock composition of juvenile materials of each type also shows distinct trends on Harker diagrams. These three chemical trends are nearly parallel, suggesting that three different magma systems were active. This is consistent with the lithic componentry showing three spatially distinct vent sources. The geological and petrological evidence is supported by a Bouguer anomaly map. Akan caldera is characterized by three circular closed minima, indicative of three depressed segments that correspond to the source regions, each of which possibly discharged the three types of magma. Caldera-forming eruptions of Akan caldera occurred from at least three distinct sources with distinct magma systems. In conclusion, Akan caldera is a composite caldera, and its shape reflects the distribution of multiple source regions.

The case study of Akan caldera shows a possible time-space evolutionary pathway for a caldera complex where several smaller calderas are nested.

KEYWORDS

composite caldera, lithic fragments, Bouguer anomaly map, magma system, Akan volcano

1 Introduction

Processes of caldera formation from explosive silicic volcanism have been well studied because of their association with large-scale and widely distributed ignimbrites, vigorous geothermal activity, mineralization, and potential to cause catastrophic damage to society on regional to global scales (Maeno and Taniguchi, 2007; Geyer and Marti, 2014; Hasegawa et al., 2016; Gooday et al., 2018; Takarada and Hoshizumi, 2020). Since the documentation of classification schemes for caldera formation under piston, piecemeal, and funnel types by Williams (1941), Williams and McBirney (1979), and Lipman (1997), many calderas have been investigated and assigned according to these categories. However, more recent studies suggest that these distinct modes of formation may be too simple in some instances. First, some calderas are geometrically complex, containing elements of more than a single structural type and formation process (Cole et al., 1998; Lipman, 2000; Acocella, 2006, 2007; Geyer and Marti, 2014). Second, the classification is generally based on the assumption that calderas are formed by eruptions from a single large magma body, but recent studies have suggested that caldera-forming eruptions may be more commonly related to multiple magma bodies (Wilson et al., 2006; Deering et al., 2007; Nakagawa et al., 2018).

The term "composite caldera" has been used for a few calderas with multiple collapse structures, especially in terms of their gravity anomaly characteristics (Hasegawa et al., 2009; Yokoyama, 2016). Yokoyama (2016) listed Aso, Aira (both are in Kyushu, Japan), and Toba (Sumatra, Indonesia) calderas as composite calderas. In addition to Aso, Aira, and Toba, Santorini caldera in the Aegean Sea, Greece (Druitt and Francaviglia, 1992), and Okataina caldera in the Taupo Volcanic Zone (TVZ), North Island, New Zealand (Jurado-Chichay and Walker, 2000), have been called "composite" due to their complex geometries. Toba and Okataina are also referred to as a "caldera complex" (Spinks et al., 2005; Chesner, 2012). Composite calderas are increasingly being linked to interactions between volcanism, regional tectonics, and multiple magma bodies (Charlier and Wilson, 2010; Fabbro et al., 2017). These calderas, without exception, formed not from a single eruption but from several eruption events, suggesting that the number and vent positions of caldera-forming eruptions are related to their formation processes.

Reconstruction of the number and source vent locations of caldera-forming eruptions is generally difficult due to thick caldera-fill deposits and, later volcanic and structural overprinting inside the caldera. This type of problem can be resolved by combining multi-disciplinary criteria, such as geophysics, geology, and geochemistry. In particular, geologic and petrologic information on lithic fragments provides a useful method for evaluating source vents (Suzuki-Kamata et al., 1993; Cole et al., 1998; Yasuda and Suzuki-Kamata, 2018). As in the abovementioned examples, gravitational surveying is also a powerful tool to remove the thick masks of caldera-filling deposits and visualize the inner caldera structure (Hasegawa et al., 2009; Yokoyama, 2016). In addition, identifying temporal geochemical changes in silicic magma systems assists to establish the complex process of caldera formation (Charlier and Wilson, 2010).

In this study, we present a comprehensive model for the formation process of Akan composite caldera, eastern Hokkaido, Japan (Figure 1). Akan caldera shows a complex geometry characterized by its irregular shape (24 × 13 km in diameter). Several distinct pyroclastic units are distributed across a wide area around the caldera (Hasegawa and Nakagawa, 2016). In order to investigate the unusual shape of this caldera, we carried out component analysis of lithic fragments in pyroclastic deposits from the caldera-forming eruptions. From the combined componentry analysis and existing Bouguer anomaly maps (Hasegawa et al., 2009), we modelled caldera-forming processes associated with the composite structure, which is composed of at least three sub-circular vent depressions. Moreover, by adding petrological constraints to the model, we show that changes in vent position were associated with renewed silicic magma system activity. The composite evolution, in time and space, of Akan caldera has broad implications for understanding the formation of calderas from a multidisciplinary perspective.

2 Geological background

2.1 General geology around Akan volcano

Akan volcano is located on the south end of the Akan-Shiretoko volcanic chain (ASVC) in the southern Kurile arc (Figures 1A,B). This part of the arc is characterized by oblique subduction of the Pacific Plate beneath the North American Plate, which began during the late Miocene (Kimura, 1986). Anticline formation and uplift of ASVC might be related to

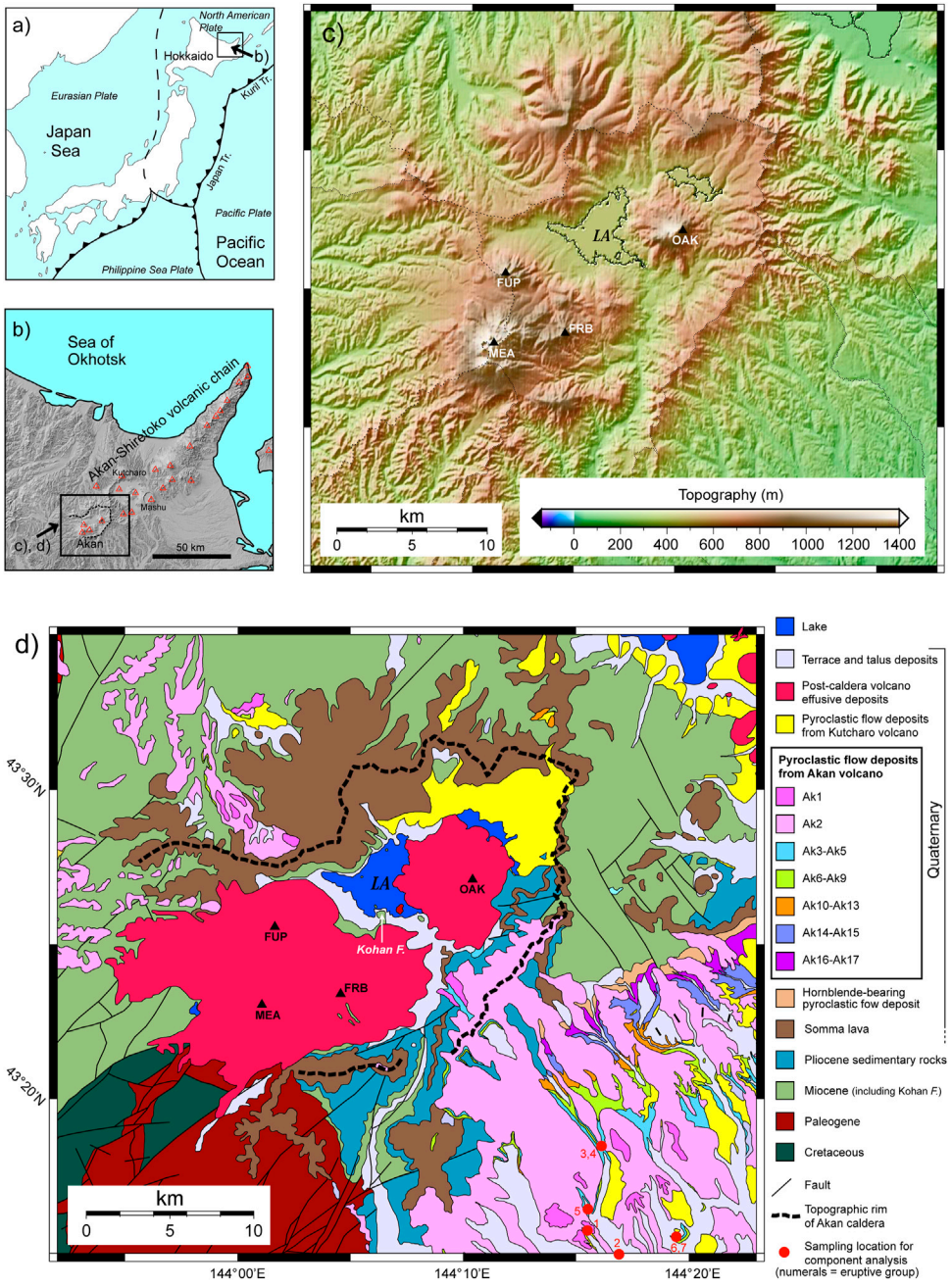

FIGURE 1
Index map around Japan **(A)**, eastern Hokkaido **(B)**, and Akan caldera **(C, D)**. **(A)** Tectonic setting around Japan Island arcs with related plates (italicized) and their boundaries. **(B)** Shaded relief map (illuminated by the light from the NW direction) of eastern Hokkaido showing Akan-Shiretoko volcanic chain composed of Quaternary volcanoes (red triangles). **(C)** Color-shaded image demonstrates digital topography of Akan caldera. **(D)** Geologic map with sampling location. It is of note that Miocene basement rock (Kohan Formation) is exposed at the center of Akan caldera. Areas of **(C)** and **(D)** are the same. Closed triangles, followed by three letters, show major named summits of post-caldera volcanoes. OAK: Mt. Oakan-dake, MEA: Mt. Meakan-dake, FUP: Mt. Fuppushi-dake, FRB: Mt. Furebetsu-dake. LA, Lake Akan.

compressional deformation associated with the westward movement of the Kurile forearc sliver (Goto et al., 2000). The basement rocks of Akan volcano consist of Cretaceous to Neogene sedimentary and volcanic rocks (Katsui, 1958). Lavas with K-Ar ages of 3.9–2.8 Ma (New Energy and Industrial Technology Development Organization, 1992; Goto et al., 2000), which constitute the caldera rim (somma lava), presumably represent pre-caldera stratovolcanoes that are

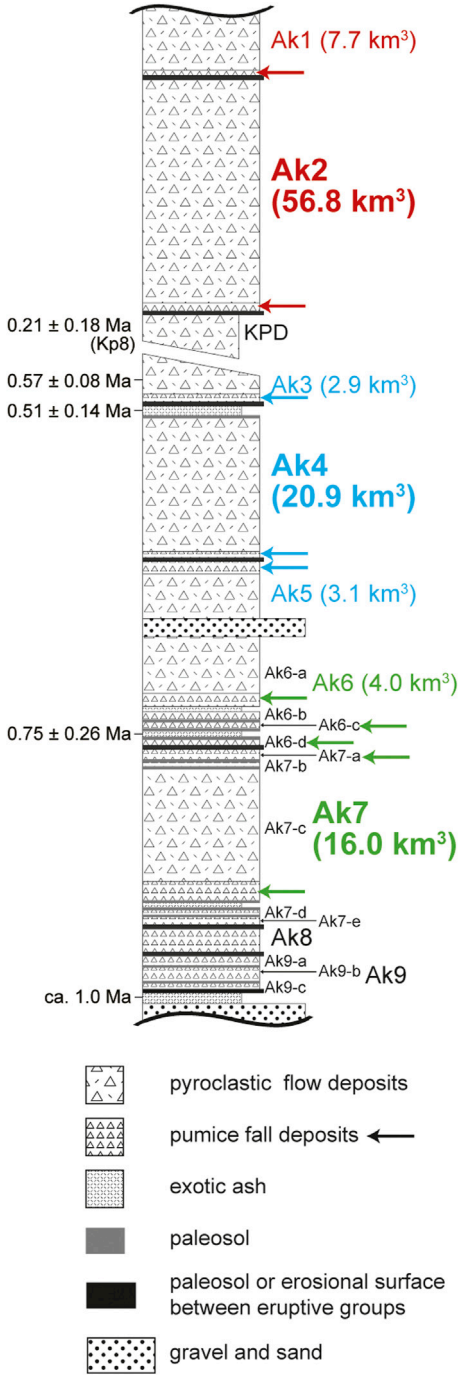

FIGURE 2
Schematic stratigraphic column of Akan pyroclastic deposits (modified from Hasegawa and Nakagawa, 2016). Sampling levels are indicated by colored arrows. Radiometric ages are measured from Kp8 (the oldest KPD: Kutcharo pyroclastic deposits), Ak3, and exotic ashes from central Hokkaido.

much older than Quaternary caldera-forming eruptive materials. It should be noted that Miocene basement rocks (Kohan Formation: Satoh, 1965) are exposed at the central portion of the caldera basin (Figure 1D), which is one of the most important characteristics of this caldera.

At least three Quaternary calderas are clustered within a 50 km^2 area at the southwestern end of ASVC. The westernmost caldera at Akan volcano (Akan caldera) is the oldest in this cluster (Katsui, 1958). Kutcharo caldera, the largest caldera in Japan at 26 × 20 km, is near the eastern side of Akan caldera. Holocene Mashu caldera is situated on the eastern rim of Kutcharo caldera. Kutcharo and Mashu calderas show normal circular shapes, whereas Akan caldera is more irregular. More than 70 large-scale Quaternary explosive eruptions (VEI >5) have been recorded from the caldera cluster (Hasegawa et al., 2012), and the estimated total bulk volume of tephra from these eruptions is approximately 1,000 km^3 (Hasegawa et al., 2012). The locus of large-scale explosive eruptions has migrated eastward from Akan to Mashu, probably due to a change in regional tectonic stress from compressional to neutral or tensional (Hasegawa and Nakagawa, 2016).

2.2 Akan pyroclastic deposits

Pyroclastic deposits related to the formation of Akan caldera (Akan pyroclastic deposits, henceforth APD) are distributed within 30 km of the caldera on its southeastern and northwestern sides (Figure 1D). Accumulations of pyroclastic flow and fall deposits more than 1,000 m thick crop out along the rivers on the southeastern side of the caldera. The APD are divided into at least 40 “eruptive units,” of which some are separated by paleosols that represent significant time intervals between eruptions. These 40 eruptive units can be summarized into 17 eruptive “groups” (Ak1–Ak17, in descending stratigraphic order), each of which is composed of a series of eruptive units (Hasegawa and Nakagawa, 2016). Akan eruptive groups are petrologically distinct based on whole-rock major element chemistry of juvenile materials (pumice and scoria), and some are intercalated with pyroclastic deposits from Kutcharo caldera (KPD) and distal air-fall ash layers from central Hokkaido (Hasegawa and Nakagawa, 2016) (Figure 2). The radiometric ages for these “exotic” tephras range from 1.4 Ma to 0.21 Ma, suggesting that the caldera-forming eruptions of the Akan volcano occurred over a period of more than one million years (Hasegawa and Nakagawa, 2016). Akan caldera can be defined as a long-lived caldera on Earth based on the worldwide collapse caldera database (http://www.gvb-csic.es/CCDB.htm).

Between the 17 eruptive groups of APD, there are relatively thick (>30 cm) paleosol layers or angular unconformities, representing relatively long dormancy periods. The time interval between Ak3 and Ak2 was especially long (around 300 kyr, Figure 2). All eruptive groups except Ak8, Ak9, and Ak11 include a pyroclastic flow deposit, and most of these are preceded by a pumice fall. The maximum grain size of lithic fragments in layer 2b (Sparks et al., 1973) of these pyroclastic flow deposits tends to increase toward the center of Akan caldera. The thicknesses of pumice fall units also increase toward Akan caldera. The total volume of APD is estimated to be approximately 170 km^3 DRE (Hasegawa and Nakagawa, 2016). Although the volumes of most eruptive groups are less than VEI 6 (10 km^3 DRE), groups Ak2, Ak4, Ak7, and Ak13 are larger than 10 km^3 DRE (VEI >6). Eruptive group Ak2 is by far the largest, at more than 55 km^3 DRE. Juvenile material in APD consists of clasts of relatively aphyric (2–17 vol% phenocrysts) white and gray pumice, with subordinate banded pumice and scoria of nearly identical mineralogy of olivine-bearing two pyroxene andesite to rhyolite.

3 Approach and methodology

In order to investigate the processes of caldera formation, we focused on the younger eruptive groups (Ak1–Ak7: ca. 0.75 to 0.20 Ma) because these are relatively large (>10 km^3 DRE) and may control the present caldera shape. We approached the main objective by analyzing the componentry of lithic fragments in APD and integrated these data with a previously reported major element (Hasegawa and Nakagawa, 2016) and newly obtained trace element compositions of juvenile materials. In combination with the Bouguer anomaly map (Hasegawa et al., 2009), this approach allowed us to discuss the number and location of vents within Akan caldera and to construct a comprehensive caldera-forming model, including the spatio-temporal evolution of the magma system.

3.1 Component analysis of lithic fragments

The general approach to determine source vent location inside a caldera is by conducting direct observations of the caldera basin (Moore and Kokelaar, 1998) or using well-defined isopach maps of pyroclastic fall deposits (Wilson et al., 2006; Jurado-Chichay and Walker, 2000). However, in the case of Akan caldera, these methods cannot be applied because it is difficult to draw detailed isopach maps due to poor exposure of deposits. Also, the caldera basin is widely covered by the products of later volcanism. In this situation, studying lithic fragments in pyroclastic deposits, composed of accessory and accidental materials from pre-existing rocks, provides a useful method for gaining information about the subsurface basement geology (Suzuki-Kamata et al., 1993; Cole et al., 1998). In order to accurately constrain vent conditions, we sampled only pyroclastic falls rather than pyroclastic flow deposits that might have entrained accidental lithics from the substrate along the flow path.

Bulk samples (1–2 kg) were collected from pumice fall units of Ak7 to Ak1 by passing through 4 mm field sieves to separate the fine component. Sampling localities and stratigraphic levels are shown in Figure 1D and Figure 2, respectively. Ak1–Ak5 are composed of single pyroclastic fall and flow deposits, whereas Ak6 and Ak7 consist of several pumice fall units each. Hence, we obtained three (Ak6-a, -c, and -d) and two (Ak7-a and -c) samples from the different pumice fall units of Ak6 and Ak7, respectively. For checking vertical variation within a single thick (>1 m) pumice fall unit, sampling levels were further subdivided into upper and lower parts for pumice fall units of Ak3, Ak6-a, and Ak7-c. Lithic fragments were picked and classified from dried bulk samples in the laboratory, and representative lithic fragments were cut for thin sectioning to verify observations made by eye and hand lens. These lithic fragments can be divided into the following ten types: porphyritic basalt (PPB), aphyric basalt (APB), porphyritic andesite (PPA), aphyric andesite (APA), dacite (DAC), diorite (DIO), welded tuff (WDT), sedimentary rock (SED), altered rock (ALT), and obsidian (OB). The highly altered nature of ALT fragments made it difficult to classify the original rock type. Proportions of these lithic types were calculated in weight percent (wt%).

Glass composition of obsidian samples was analyzed using the SEM-EDS system (JEOL JSM-T330A + LINK ISIS) at Hokkaido University (HU) to evaluate whether they represent juvenile material or not. Operating parameters were set at 15 kV for the accelerating voltage, with a beam diameter of 5 μm and a count rate of 2.0 kcps for 180 s. Corrections of the analyses were made according to the ZAF method. Total sums of major elements were 94–100 wt% and normalized to 100 wt% anhydrous on diagrams.

3.2 Geochemistry

Hasegawa and Nakagawa (2016) reported whole-rock major element chemical data for juvenile materials of APD. Here, we used those data and additional trace element data obtained through X-ray fluorescence (XRF) using a PANalytical Magix Pro at HU. Samples of fresh juvenile materials were washed, dried, and then powdered using an agate mill. In the case of units containing small-sized pumice or scoria, several clasts (>2 cm in diameter) were combined to make powder for a glass bead. Glass beads were prepared following the general methods (glass bead method, 1:2 in

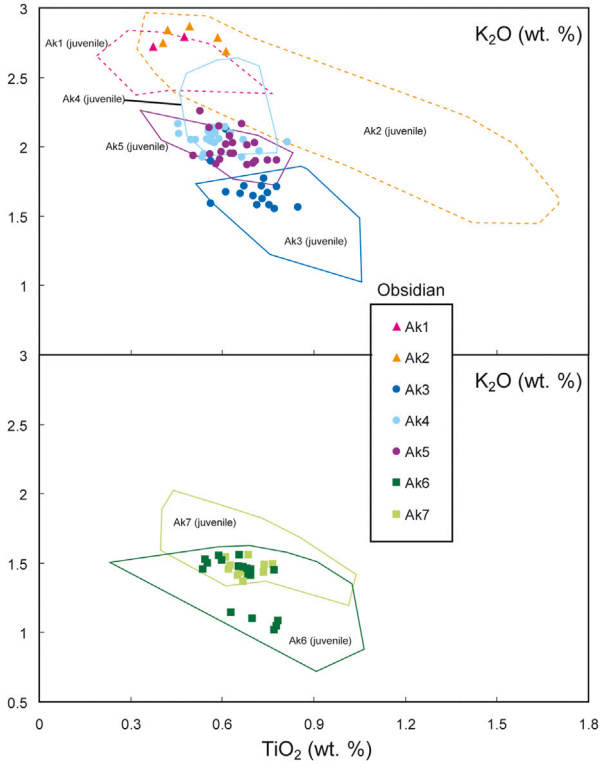

FIGURE 3
K_2O vs. SiO_2 variation diagram of glass chemistry of obsidian clasts in Ak1–Ak7, measured by SEM-EDS system. Compositional fields of juvenile materials (pumice and scoria) are from Hasegawa and Nakagawa (2016).

dilution) (Hasegawa and Nakagawa, 2016). Values for loss-on-ignition (LOI) were determined by weight loss after fusing at 800°C for 2 h. Samples with high LOI values (>6 wt%) were not used. Trace elements, including rare earth elements (REE) and Hf, Cs, Th, U, and Sc Co, were also determined *via* Thermo Fisher Scientific X-series inductively coupled plasma-mass spectrometry (ICP-MS) at HU selectively for the most silicic samples for each unit using the same powder. The analytical procedure employed for ICP-MS is based on the method of Eggins et al. (1997). A single solution of USGS reference material, BHVO-2, was used as an external calibration standard. Obtained geochemical data are shown in Supplementary Appendix A1.

3.3 Gravity survey

Hasegawa et al. (2009) carried out gravitational surveys in and around Akan caldera, including the frozen caldera lake and mountainous areas. In addition, they applied lake water corrections to generate an accurate gravity anomaly map of the caldera (Hasegawa et al., 2009). In this study, we drew a new colored-Bouguer anomaly map with an assumed reduction density of 2.4×10^3 kg/m^3, which is the median value of actual densities of basement rocks of Akan volcano (NEDO, 1992). The study by Hasegawa et al. (2009) should be referred to for more detail regarding the methods and dataset. Mass deficiency due to caldera-filling low-density materials was also calculated based on the new Bouguer anomaly map by using Gauss' theorem (Yokoyama 1958).

4 Results

4.1 Component analysis of lithic fragments and glass chemistry of obsidian clasts

All sampled units contain more or less (0.05–67.01 wt%) obsidian clasts. According to the results of SEM-EDS analysis, most obsidian clasts show the same compositions as co-existing juvenile materials (Figure 3). These data suggest that most obsidians are cognate lithic fragments (i.e., juvenile materials). Thus, we removed the fraction of obsidian (OB) from the following result of component analysis to focus on accessory and accidental materials. Figure 4 shows pie diagrams and photographs of rock-type proportions of lithics fragments in pumice fall deposits of Ak1–Ak7, after excluding OB. Characteristics of each unit are summarized as follows:

4.1.1 Ak7

Although there is a slight vertical variation of proportions, the componentry of lithic fragments of lower and upper parts in pumice fall of Ak7-c is approximately the same. Dominant lithic fragments in Ak7-c are APA (45%–47%), followed by ALT (25%–26%). DAC (13%) and PPB (4%–6%) are also common. Smaller quantities of WDT (1%–4%), SED (2%), PPA (2%–3%), and APB (2%) occur. The most common lithic fragments of Ak7-a are still APA (41%) and ALT (37%) with subordinate DAC (10%). In addition to these major components, assemblages of other minor components are the same as those of Ak-7c.

4.1.2 Ak6

Most lithic fragments in pumice fall deposits of Ak6-c and Ak6-d are APA (38%–55%) and ALT (30%–41%) with subordinate DAC (6%–8%). Minor components are also common as SED (1%–4%), APB (2%–3%), PPA (2%–3%), PPB (1%–3%), and WDT (1%–2%). The lithic components of upper parts in pumice fall of Ak6-a are poorer in DAC (5%) than in the lower part (11%). However, both upper and lower parts are commonly dominant in APA (46%) and ALT (36%–37%), which represents the general componentry in Ak6.

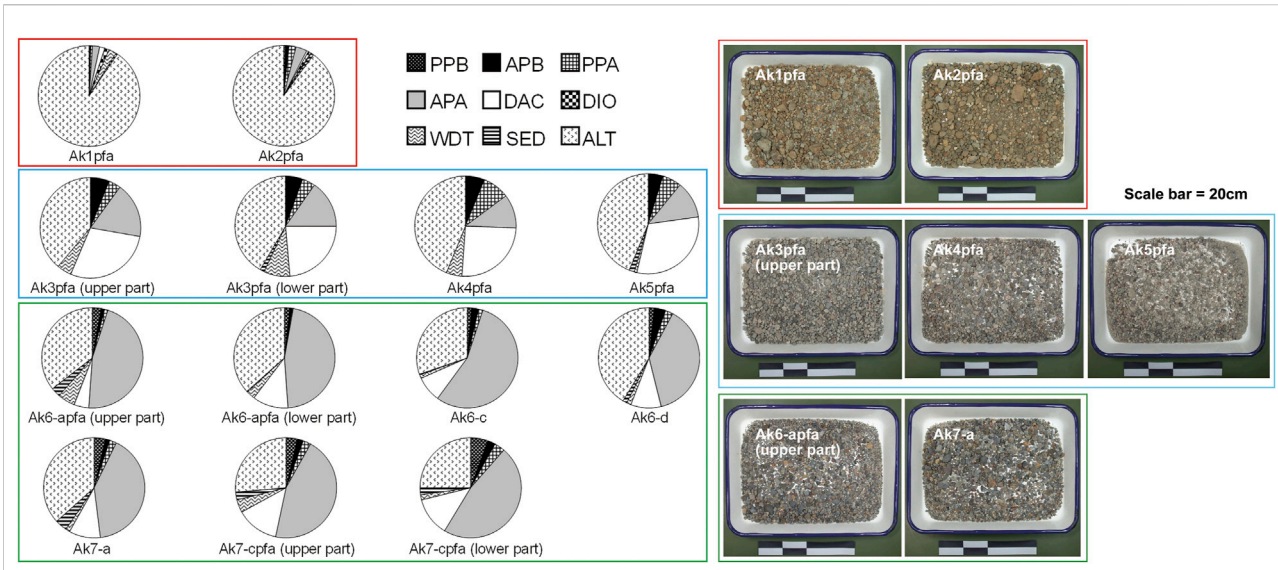

FIGURE 4
Photographs (right) and pie diagrams (left) showing relative proportions of lithic fragment types in each unit. Type A, B, and C (see main text) are enclosed by red, blue, and green boxes, respectively.

4.1.3 Ak5

The most common lithic fragment type in pumice fall of Ak5 is ALT (44%), followed by DAC (31%). Subsequently, APA (12%), PPA (6%), and APB (5%) are recognized with minor amounts of SED (2%) and WDT (1%). PPB is lacking in Ak5.

4.1.4 Ak4

Most lithic components in pumice fall of Ak4 are ALT (44%) and DAC (25%). Also, APA (11%), PPA (8%), APB (6%), and WDT (5%) are recognized, but PPB is not recognized in Ak4.

4.1.5 Ak3

ALT (38%) and DAC (29%) are the most common lithic component in pumice fall of Ak3 throughout the lower and upper parts. Commonly, APA is a subordinate component (14%) with a smaller amount of WDT (5%–8%), APB (5%), and PPA (4%). PPB fragments are commonly absent in Ak3. Furthermore, there is no SED in the upper part.

4.1.6 Ak2

Ak2 is characterized by a considerably larger quantity of ALT (90%). DIO, which is lacking in Ak3–Ak7, is also recognized in Ak2.

4.1.7 Ak1

The most dominant lithic component in pumice fall of Ak1 is ALT (91%). DIO is also included in Ak1.

On the basis of componentry of lithic fragments and stratigraphic sequence, we grouped Ak1–Ak7 into the following three types: type A (Ak1 and Ak2: youngest), type B (Ak3–Ak5), and type C (Ak6 and Ak7: oldest). The dominant and characteristic lithic component in type A is ALT (>90 wt%). Although ALT consists of a variety of highly altered rocks, it is indicative of hydrothermal (fumarole) alteration and/or oxidation in the presence of a significant hydrothermal system at the vent area. DIO is minor but also a characteristic component in type A. Type B is commonly rich in ALT (38%–44%) with subordinate amounts of DAC (25%–31%) but characteristically lacking in PPB, which is recognized in types A and C. In type C, APA (38%–55%) is the most common lithic component, followed by ALT (25%–41%) and DAC (5%–13%).

The similarity of lithic components within one type indicates that the vent areas providing the eruption deposits were the same or very close to each other (Cole et al., 1998). Glass chemistry data of obsidian clasts also support this view (Figure 3). Although analyzed obsidians are mostly juvenile, some accessory obsidian clasts can be identified based on their chemical compositions. In the case of Ak3, most obsidian clasts plot in the compositional field of juvenile materials, but two obsidian fragments correspond to the compositional area of juveniles of Ak4 (and Ak5). This implies that Ak3 eruption occurred at the same vent area as Ak4/5 and then destroyed and incorporated pre-existing obsidian products (e.g., lava dome) that were formed by the previous activity of Ak4/Ak5. Similar compositional relationships are recognized between Ak6 and Ak7. Glassy

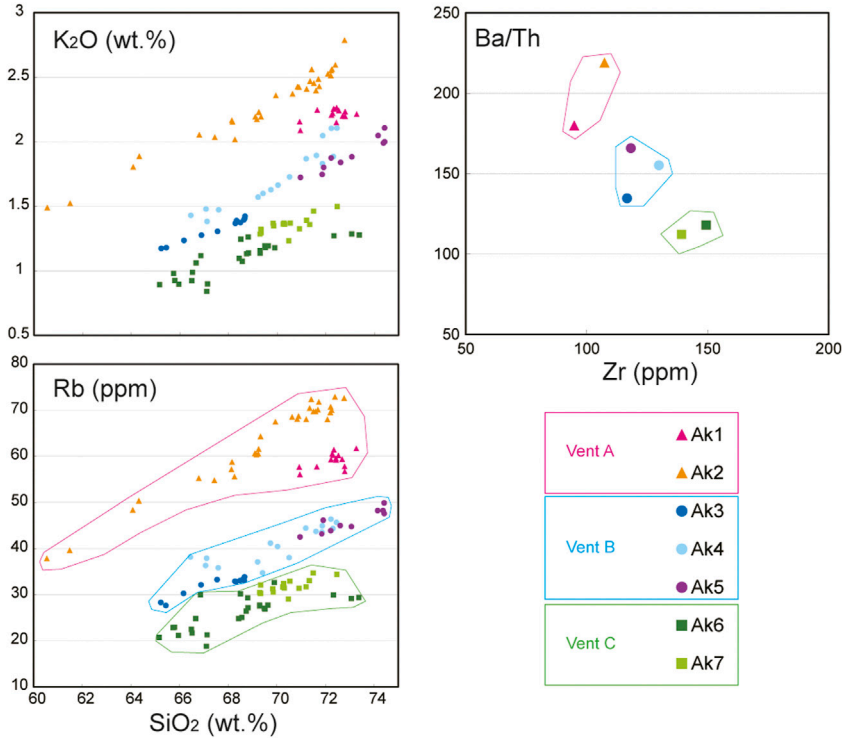

FIGURE 5
Selected diagrams of whole-rock chemistry for juvenile materials of A1–Ak7.

obsidian lava may have been generated with Plinian eruptions and was destroyed by later explosive volcanism at the same vent area. Vent systems ejecting through Ak7–Ak1 were composed of at least three distinct regions, each of which successively repeated a couple of Plinian eruptions with contemporaneous obsidian lava effusion.

4.2 Chemistry

As concluded in Hasegawa and Nakagawa (2016), the magma systems of each eruptive group were independent. The whole-rock chemistry of Ak1–Ak7 is characterized by a wide variation of K_2O (0.8–2.8 wt%) and Rb (18–75 ppm) contents within a narrow range of SiO_2 (65–75 wt%) (Figure 5). On a SiO_2 vs. K_2O diagram, each group forms a distinct, compact or elongated cluster. This suggests that these diverse magmas were not emplaced through a single, large magma chamber but rather were generated independently, existed separately, and erupted sequentially from their own magma chambers beneath the 24 × 13 km area of Akan caldera. The existence of banded pumice, along with the linear trends of the eruptive groups on chemical variation diagrams, suggest that magma mixing was a common process in each group (Hasegawa and Nakagawa, 2016). Furthermore, the linear, subparallel trends on the K_2O- and Rb-SiO_2 diagrams indicate that both mafic and silicic components were independent in each eruptive group.

4.3 Gravitational structure of Akan caldera

A new colored Bouguer anomaly map of Akan caldera after lake-water correction is shown in Figure 6A. It is of note that considerably high (>100 mGal) and low (<50 mGal) gravity regions are widely recognized in the south and north parts of Akan caldera, respectively. The former reflects the distribution of Paleogene basement rocks that comprise the anticline structure of ASVC, whereas the latter corresponds to the sedimentary basin on the north side of the anticline. Inside Akan caldera, an E-W trending (20 km wide and 10 km lengthwise) low gravity zone can be identified that is indicative of a caldera basin. The low gravity zone is surrounded by closely-spaced contour lines that lie significantly (>1 km) inside the topographic rim of Akan caldera (white dashed line). Closely-spaced contour lines in

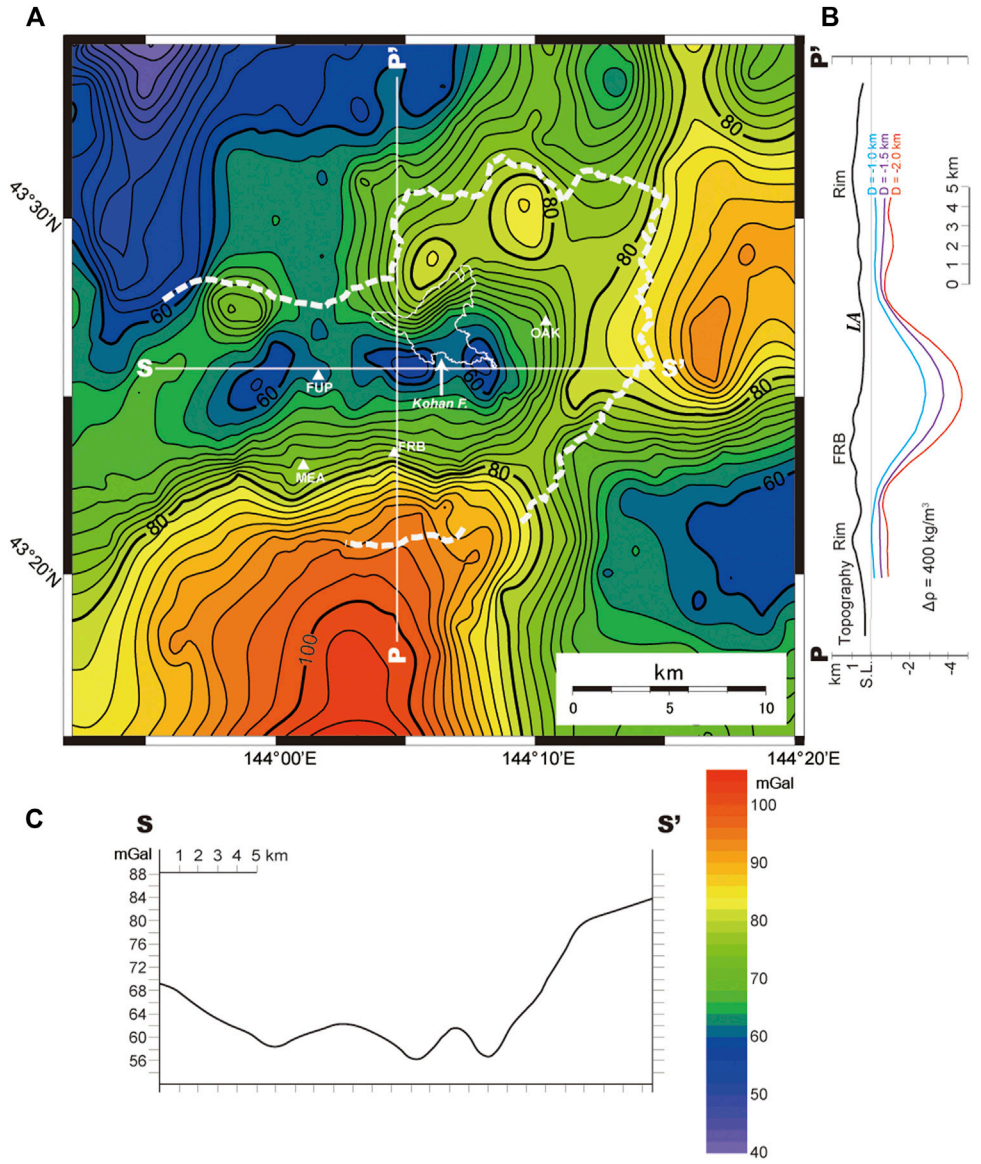

FIGURE 6
(A) Colored Bouguer anomaly maps of Akan volcano after the lake water correction, with contour intervals of 2 mGal. Reduction density is 2,400 kg m^{-3}. Dashed white line indicates the topographic rim of Akan caldera. Thin white line indicates the coastline of Lake Akan (LA). The same point of distribution of Miocene Kohan Formation (F.) as Figure 1 is indicated by an arrow. The caption of Figure 1 should be referred to for the abbreviations of post-caldera volcanoes (white triangles). **(B)** Profiles of the residual gravity anomalies, topography, and deduced subsurface structure along P-P′ in **(A)** (Modified from Figure 8 from Ohkawa and Yokoyama, 1979). D denotes the mass condensation depth adopted in the sin x/x method. **(C)** Cross-section of Bouguer anomaly along S-S′ in **(A)**.

Bouguer anomaly maps generally indicate a large density gradient. Thus, the contour lines (70–80 mGal) correspond to the bounding faults associated with caldera collapse (Lipman, 1997). The major trend of the E-W trending caldera bounding fault is consistent with the direction of local faulting in this area (Figure 1D), implying that the outline of Akan caldera might be more or less controlled by pre-existing faults. The disagreement between the bounding fault (structural rim) and topographic rim of Akan caldera indicates that the present rim has been expanded more than 1 km outside after the caldera-formation. Post-caldera volcanoes, except for Fuppushi-dake (FUP), are located along the closely-spaced contour lines, suggesting that these post-caldera volcanoes lie along the bounding faults associated with caldera collapse.

The difference between the maximum and minimum Bouguer anomaly values from the structural rim (80–mGal) to the bottom of Akan caldera (ca. 55 mGal) is approximately 25– mGal. This value is lower than that of the adjacent Kutcharo caldera (40– mGal: Yokoyama, 1958; Ichihara et al., 2009) situated on the same tectonic setting as Akan caldera. Ohkawa and Yokoyama (1979) roughly deduced the subsurface structure of Akan caldera based on residual gravity anomalies and the two-dimensional sin x/x method (calculating the subterranean mass distribution of a plane on which the mass is assumed to be condensed and responsible for observed gravity anomalies), and the maximum bottom depth of which was estimated to be around 2.7–4.7 km from sea level (Figure 6B). The estimated bottom depth of the Kutcharo caldera basin has a similar value of 3.5 km or more (Ichihara et al., 2009). In this study, we calculated mass deficiency due to the low-density materials based on the new Bouguer anomaly map by using Gauss' theorem (Yokoyama 1958) and obtained a mass deficiency of 5.3×10^{10} tons. This value is consistent with the results of Ohkawa and Yokoyama (1979). Taking the density difference between basement and caldera-filling low-density materials to be 400 kg/m^3 by Ohkawa and Yokoyama (1979), the bulk volume of caldera-fill can be calculated to be 131 km^3. This shows mostly good agreement with the geologically estimated volume of APD (170 km^3 DRE) from Hasegawa and Nakagawa (2016).

Figure 6C shows an E-W Bouguer anomaly cross-section for Akan caldera. The figure emphasizes the three individual depressions with inverted cone shapes, each of which is around 3–5 km in diameter. The three circular closed minima in the Bouguer anomaly map suggest that at least three major depressed segments filled with low-density materials exist inside Akan caldera.

5 Discussion: Time and space evolution of Akan composite caldera

Here, we discuss the spatio-temporal evolution of Akan caldera by combining the results of component analysis (see Section 4.1), magma compositions (Section 4.2), and the new Bouguer anomaly map (Section 4.3). At first, the identification of three different lithic componentry types (Figure 4) suggests that the eruptions producing types A, B, and C were derived from distinct plumbing systems. It seems that the geology of the pre-caldera volcanic field was not homogeneous, and eruptions of Ak7–Ak1 were sourced from three vent areas with different geologies. Akan caldera was formed by successive Plinian eruptions that were derived from at least three spatially distinct areas in the three discrete periods from 0.75 to 0.20 Ma. The largest eruptions (>10 km^3 DRE) during each period (Ak2 in type A, Ak4 in type B, and Ak7-c in type C) might have contributed to the caldera formation at each vent area. Vent positions of the three types (type A–type C) cannot be determined because it is difficult to correlate the lithologies between the lithic fragments and sub-surface basement rocks. However, it is speculated that the vent of type A (Ak1 and Ak2) and type C (Ak6 and Ak7) were situated in the western and eastern areas of Akan caldera, respectively. In the western area of the caldera, pyroclastic flow deposits of Ak1 and 2 are widely and thickly distributed (Figure 1D). Proximal facies of Ak2, including many altered lithic fragments, are recognized in the western area. On the other hand, isopach maps of pumice fall deposits in Ak6 and Ak7 converge to the eastern area of Akan caldera, indicative of an eastern source vent (Hasegawa and Nakagawa, 2016).

In order of increasing K_2O and Rb contents, juvenile materials from types C, B, and A deposits form three distinct trends (Figure 5). These data suggest that magma systems were renewed during the transitional periods from type C to type B (from Ak6 to Ak5) and type B to type A (Ak3 to Ak2). The geochemical features are consistent with the results of lithic component analysis, which implies distinct vent areas for types C, B, and A deposits. During the deposition of Ak7–Ak1, thick beds of gravel and sand (>2 m) separated Ak6 and Ak5, and a prolonged (>300 kyr) dormancy period existed between Ak3 and Ak2 (Figure 2). Furthermore, the Kutcharo volcano to the east started caldera-forming activity during the period between Ak3 and Ak2. For the successive eruption groups, the development of new magma systems that sourced different vent areas may have taken long time periods. On the other hand, magmas derived from the same (or very close) vent areas, such as Ak6/Ak7 in type C and Ak3/4/5 in type B, show similar compositions, suggesting silicic magmas from the same source were active in the same area. Thus, distinct silicic magma systems were active during three discrete periods at different areas in the Akan volcano from approximately 0.75 Ma (Ak7) to 0.20 Ma (Ak1). More detailed (ongoing) work is required to investigate whether these chemical variations can be explained by different degrees of partial melting from a single source.

The Bouguer anomaly map suggests at least three major depressed segments inside Akan caldera (Figures 6A and C). We infer that these three depression centers correspond to the three vent areas, each of which is related to the three types of lithic componentry and magmas. Between the eastern two circular minima of the Bouguer anomaly map, there exists the exposure of Miocene basement rock (Kohan Formation) at the center of the bottom of Akan caldera (Figure 6A). Generally speaking, pre-caldera basement rocks are hardly exposed in the bottom center of low gravity type calderas. This exposure of basement rock inside Akan caldera is thought to be a part of a remnant caldera rim structure separating the eastern two small depressions. We are aware of an example of remnant

pre-caldera volcanic edifice (Neko-dake) that is situated inside Aso composite caldera, Kyushu, Japan (Yokoyama, 2016). As mentioned earlier, post-caldera volcanoes, except Fuppushi-dake (FUP), are situated on closely spaced contour lines of Bouguer anomaly, which reflect the bounding faults associated with the caldera collapse. Only Fuppushi-dake is situated between the western two circular minima, which might have been generated along the bounding fault associated with the western two caldera collapse structures. Therefore, Akan caldera can be considered a composite caldera composed of three relatively small source vents along 20 km in an E-W direction.

On the basis of detailed geological, geophysical and geochemical data, we conclude that Akan caldera defines a case-type of a multi-cyclic composite caldera composed of at least three spatially and temporally distinct small calderas. A combination of multidisciplinary data has revealed the coupling of changes in vent areas and magma systems. The E-W elongated shape of Akan caldera reflects the distribution of multiple vent areas that were connected to multiple magma bodies. Caldera collapse controlled by local faults and post-collapse erosion/elongation of the caldera rim might have finally contributed to the irregular shape (Belousov et al., 2005; Maestrelli et al., 2021). The adjacent Kutcharo and Mashu calderas show normal circular shapes in contrast to Akan caldera (Figure 1B), despite the same stress field.

Composite calderas on Earth listed in chapter one, such as Akan, Aso, Aira, Toba, Santorini, and Okataina, are commonly situated on arc-trench systems, implicating that geological setting is important to determine the style of caldera-forming eruptions and processes. Compared to these composite calderas, Akan is characterized by long life (>1 million years from Ak17 to Ak1) and diverse magma compositions (e.g., K_2O = 0.8–2.8 wt% with a narrow range of SiO_2: Figure 5). The diversity of Akan magma almost equals that of a combination of Kutcharo and Mashu magmas from medium- to low-K_2O rock series (Hasegawa et al., 2012: Hasegawa and Nakagawa, 2016).

6 Conclusion

By combining the results of component analysis of lithic fragments in pumice fall deposits, petrological and geochemical analyses of juvenile materials and gravity survey, the formation process of Akan caldera was comprehensively revealed. The conclusions of this study are summarized as follows:

(1) During the younger caldera-forming activity of Akan volcano (Ak7–Ak1: ca. 0.75–ca. 0.20 Ma), large-scale Plinian eruptions occurred from at least three different vent areas.
(2) The vent areas migrated during the periods from Ak6 to Ak5 and from Ak3 to Ak2.
(3) The migrations were accompanied by considerable changes to the compositions of the silicic magmas that fed the corresponding eruptions.
(4) Akan caldera can be defined as a typical "composite caldera", whose irregular, E-W elongated shape reflects the distribution of three relatively small calderas constrained by geology, gravity, and chemistry.

This study has outlined a detailed scenario by which a composite caldera was constructed *via* the formation of several nested caldera volcanoes. The complex and long-term caldera-formation model of Akan volcano contributes to the understanding of other terrestrial caldera formation processes and structures which may have been oversimplified.

Data availability statement

The original contributions presented in the study are included in the article/Supplementary Material; further inquiries can be directed to the corresponding author.

Author contributions

TH performed all the geological, petrological, and gravitational works and wrote the manuscript. MN performed the geological survey and designed the study. HK performed the gravitational survey and interpreted the data. AY supervised the gravitational study.

Funding

This research was partly supported by Fukada Grant-in-Aid from Fukada Geological Institute, the charitable trust Moriyasu Graduate Student Grant, JSPS KAKENHI Number JP16K01311, JP16KK0092, JP17K05683 (TH), and MEXT Integrated Program for Next Generation Volcano Research and Human Resource Development.

Acknowledgments

We wish to express our gratitude to the two reviewers for their helpful comments, and to Chris Conway (Geological Survey of Japan) for proofreading the manuscript.

Conflict of interest

Author HK was employed by Ueyama-Shisui Co., Ltd.

The remaining authors declare that the research was conducted in the absence of any commercial or financial relationships that could be construed as a potential conflict of interest.

Publisher's note

All claims expressed in this article are solely those of the authors and do not necessarily represent those of their affiliated organizations, or those of the publisher, the editors, and the reviewers. Any product that may be evaluated in this article, or claim that may be made by its manufacturer, is not guaranteed or endorsed by the publisher.

Supplementary material

The Supplementary Material for this article can be found online at: https://www.frontiersin.org/articles/10.3389/feart.2022.953152/full#supplementary-material

References

Acocella, V. (2006). Caldera types: How end-members relate to evolutionary stages of collapse. *Geophys. Res. Lett.* 33, L18314. doi:10.1029/2006gl027434

Acocella, V. (2007). Understanding caldera structure and development: An overview of analogue models compared to natural calderas. *Earth. Sci. Rev.* 85, 125–160. doi:10.1016/j.earscirev.2007.08.004

Belousov, A., Walter, T. R., and Troll, V. R. (2005). Large-scale failures on domes and stratocones situated on caldera ring faults: Sand-box modeling of natural examples from kamchatka, Russia. *Bull. Volcanol.* 67, 457–468. doi:10.1007/s00445-004-0387-1

Charlier, B. L. A., and Wilson, C. J. N. (2010). Chronology and evolution of caldera-forming and post-caldera magma systems at Okataina volcano, New Zealand from zircon U-Th model-age spectra. *J. Petrology* 51, 1121–1141. doi:10.1093/petrology/egq015

Chesner, C. A. (2012). The Toba caldera complex. *Quat. Int.* 258, 5–18. doi:10.1016/j.quaint.2011.09.025

Cole, J. W., Brown, S. J. A., Burt, R. M., Beresford, S. W., and Wilson, C. J. N. (1998). Lithic types in ignimbrites as a guide to the evolution of a caldera complex, Taupo volcanic centre, New Zealand. *J. Volcanol. Geotherm. Res.* 80, 217–237. doi:10.1016/s0377-0273(97)00045-0

Deering, C. D., Vogel, T. A., Patino, L. C., and Alvarado, G. E. (2007). Origin of distinct silicic magma types from the Guachipelin caldera, NW Costa Rica: Evidence for magma mixing and protracted subvolcanic residence. *J. Volcanol. Geotherm. Res.* 165, 103–126. doi:10.1016/j.jvolgeores.2007.05.004

Druitt, T. H., and Francaviglia, V. (1992). caldera formation on Santorini and the physiography of the islands in the late bronze age. *Bull. Volcanol.* 54, 484–493. doi:10.1007/BF00301394

Eggins, S. M., Woodhead, J. D., Kinsley, L. P. J., Mortimer, G. E., Sylvester, P., and McCulloch, M. T. (1997). A simple method for the precise determination of ≥40 trace elements in geological samples by ICPMS using enriched isotope internal standardisation. *Chem. Geol.* 134, 311–326. doi:10.1016/S0009-2541(96)00100-3

Fabbro, G. N., Druitt, T. H., and Costa, F. (2017). Storage and eruption of silicic magma across the transition from dominantly effusive to caldera-forming states at an arc volcano (Santorini, Greece). *J. Petrology* 58, 2429–2464. doi:10.1093/petrology/egy013

Geyer, A., and Marti, J. (2014). A short review of our current understanding of the development of ring faults during collapse caldera formation. *Front. Earth Sci. (Lausanne).* 2, 22. doi:10.3389/feart.2014.00022

Gooday, R. J., Brown, D. J., Goodenough, K. M., and Kerr, A. C. (2018). A proximal record of caldera-forming eruptions: The stratigraphy, eruptive history and collapse of the palaeogene arran caldera, Western scotland. *Bull. Volcanol.* 80 (9), 70. doi:10.1007/s00445-018-1243-z

Goto, Y., Funayama, A., Gouchi, N., and Itaya, T. (2000). K-Ar ages of the Akan-Shiretoko volcanic chain lying oblique to the Kurile trench: Implications for tectonic control of volcanism. *Isl. Arc* 9, 204–218. doi:10.1046/j.1440-1738.2000.00273.x

Hasegawa, T., Yamamoto, A., Kamiyama, H., and Nakagawa, M. (2009). Gravity structure of Akan composite caldera, eastern Hokkaido, Japan: Application of lake water corrections. *Earth Planets Space* 61, 933–938. doi:10.1186/bf03353205

Hasegawa, T., Matsumoto, A., and Nakagawa, M. (2016). Evolution of the 120 ka caldera-forming eruption of Kutcharo volcano, eastern Hokkaido, Japan: Geologic and petrologic evidence for multiple vent systems and rapid generation of pyroclastic flow. *J. Volcanol. Geotherm. Res.* 321, 58–72. doi:10.1016/j.jvolgeores.2016.04.030

Hasegawa, T., Nakagawa, M., and Kishimoto, H. (2012). The eruption history and silicic magma systems of caldera-forming eruptions in eastern Hokkaido, Japan. *J. Mineralogical Petrological Sci.* 107, 39–43. doi:10.2465/jmps.111020h

Hasegawa, T., and Nakagawa, M. (2016). Large scale explosive eruptions of Akan volcano, eastern Hokkaido, Japan: A geological and petrological case study for establishing tephro-stratigraphy and -chronology around a caldera cluster. *Quat. Int.* 398, 39–51. doi:10.1016/j.quaint.2015.07.058

Ichihara, H., Mogi, T., Hase, H., Watanabe, T., and Yamaya, Y. (2009). Resistivity and density modelling in the 1938 Kutcharo earthquake source area along a large caldera boundary. *Earth Planets Space* 61, 345–356. doi:10.1186/bf03352916

Jurado-Chichay, Z., and Walker, G. P. L. (2000). Stratigraphy and dispersal of the Mangaone Subgroup pyroclastic deposits, Okataina volcanic centre, New Zealand. *J. Volcanol. Geotherm. Res.* 104, 319–380. doi:10.1016/s0377-0273(00)00210-9

Katsui, Y. (1958). Akan and Kutcharo volcanoes. *Chikyu Kagaku (Earth Sci.)* 39, 19–29. (in Japanese). doi:10.15080/agcjchikyukagaku.1958.39_19

Kimura, G. (1986). Oblique subduction and collision: Forearc tectonics of the Kuril Arc. *Geology* 14, 404–407. doi:10.1130/0091-7613(1986)14<404:OSACFT>2.0.CO;2

Lipman, P. W. (2000). *Calderas. Encyclopedia of volcanoes*. San Francisco: Academic Press, 643–662.

Lipman, P. W. (1997). Subsidence of ash-flow calderas: Relation to caldera size and magma-chamber geometry. *Bull. Volcanol.* 59, 198–218. doi:10.1007/s004450050186

Maeno, F., and Taniguchi, H. (2007). Spatiotemporal evolution of a marine caldera-forming eruption, generating a low-aspect ratio pyroclastic flow, 7.3 ka, kikai caldera, Japan: Implication from near-vent eruptive deposits. *J. Volcanol. Geotherm. Res.* 167, 212–238. doi:10.1016/j.jvolgeores.2007.05.003

Maestrelli, D., Corti, G., Bonini, M., Montanari, D., and Sani, F. (2021). Caldera collapse and tectonics along the main Ethiopian rift: Reviewing possible relationships. *Comptes Rendus. Geosci.* 353 (S2), 91–109. doi:10.5802/crgeos.63

Moore, I., and Kokelaar, P. (1998). Tectonically controlled piecemeal caldera collapse: A case of Glencoe volcano, Scotland. *Geol. Soc. Amer. Bull.* 110, 1448–1466. doi:10.1130/0016-7606(1998)110<1448:TCPCCA>2.3.CO;2

Nakagawa, M., Amma-Miyasaka, M., Tomijima, C., Matsumoto, A., and Hase, R. (2018). Eruption sequence of the 46 ka caldera-forming eruption of shikotsu volcano, inferred from stratigraphy of proximal deposits at south of Lake shikotsu, Japan. *J. Geogr. Zasshi).* 127, 247–271. doi:10.5026/jgeography.127.247

NEDO (New Energy and Industrial Technology Development Organization) (1992). Report of Geothermal development promotion survey, 26, Akan area. 1133 (in Japanese)

Ohkawa, S., and Yokoyama, I. (1979). Subsurface structure of Akan caldera based on gravity anomalies. *Geophys. Bull. Hokkaido Univ.* 38, 17–29. doi:10.14943/gbhu.38.17

Satoh, H. (1965). Explanatory text of the geological map of Japan, scale 1: 50,000, "Akan-ko". 82, Geological Survey of Japan (in Japanese with English Abstract).

Sparks, R. S. J., Self, S., and Walker, G. P. L. (1973). Products of ignimbrite eruptions. *Geology* 1, 115–118. doi:10.1130/0091-7613(1973)1<115:POIE>2.0.CO;2

Spinks, K., Acocella, V., Cole, J., and Bassett, K. (2005). Structural control of volcanism and caldera development in the transtensional Taupo Volcanic Zone, New Zealand. *J. Volcanol. Geotherm. Res.* 144, 7–22. doi:10.1016/j.jvolgeores.2004.11.014

Suzuki-Kamata, K., Kamata, H., and Bacon, C. R. (1993). Evolution of the caldera-forming eruption at Crater Lake, Oregon, indicated by component analysis of lithic fragments. *J. Geophys. Res.* 98, 14059–14074. doi:10.1029/93jb00934

Takarada, S., and Hoshizumi, H. (2020). Distribution and eruptive volume of aso-4 pyroclastic density current and tephra fall deposits, Japan: A M8 super-eruption. *Front. Earth Sci. (Lausanne).* 8, 170. doi:10.3389/feart.2020.00170

Williams, H. (1941). Calderas and their origin. *Bull. Dep. Geol. Sci.* 25, 239–346. doi:10.2307/210295

Williams, H., and McBirney, A. R. (1979). *Calderas and cauldrons*. Volcanology. CA: Freeman, Cooper and Co.San Francisco Publ.

Wilson, C. J. N., Blake, S., Charlier, B. L. A., and Sutton, A. N. (2006). The 26·5 ka oruanui eruption, Taupo volcano, New Zealand: Development, characteristics and evacuation of a large rhyolitic magma body. *J. Petrology* 47, 35–69. doi:10.1093/petrology/egi066

Yasuda, Y., and Suzuki-Kamata, K. (2018). The origin of a coarse lithic breccia in the 34 ka caldera-forming Sounkyo eruption, Taisetsu volcano group, central Hokkaido, Japan. *J. Volcanol. Geotherm. Res.* 357, 287–305. doi:10.1016/j.jvolgeores.2018.04.017

Yokoyama, I. (1958). Gravity survey on kuttyaro caldera lake. *JPhysEarth.* 6, 75–79. doi:10.4294/jpe1952.6.75

Yokoyama, I. (2016). Origin of calderas: Discriminating between collapses and explosions. *Ann. Geophys.* 59–6. doi:10.4401/ag-7010